Whole-Body Diffusion-weighted MR Imaging in Cancer: Current Status and Research Directions[1]

Anwar R. Padhani, MB, BS, FRCP, FRCR
Dow-Mu Koh, MD, MRCP, FRCR
David J. Collins, BA, MInstP

Diffusion-weighted (DW) magnetic resonance (MR) imaging is emerging as a powerful clinical tool for directing the care of patients with cancer. Whole-body DW imaging is almost at the stage where it can enter widespread clinical investigations, because the technology is stable and protocols can be implemented for the majority of modern MR imaging systems. There is a continued need for further improvements in data acquisition and analysis and in display technologies. Priority areas for clinical research include clarification of histologic relationships between tissues of interest and DW MR imaging biomarkers at diagnosis and during therapy response. Because whole-body DW imaging excels at bone marrow assessments at diagnosis and for therapy response, it can potentially address a number of unmet clinical and pharmaceutical requirements. There are compelling needs to document and understand how common and novel treatments affect whole-body DW imaging results and to establish response criteria that can be tested in prospective clinical studies that incorporate measures of patient benefit.

Supplemental material: *http://radiology.rsna.org/lookup/suppl/doi:10.1148/radiol.11110474/-/DC1*

Online CME
See www.rsna.org/ry_cme.html

Learning Objectives:

- Recognize the biophysical tissue properties that are informed by diffusion-weighted (DW) MR imaging, and how normal tissues show impeded diffusion.
- Review causes of marrow hypoplasia and hyperplasia and of false-positive and false-negative results in lesion detection, as well as how these affect bone marrow signal intensity on DW MR images.
- Discuss DW MR changes in response to therapy and how this can be assessed.

Accreditation and Designation Statement

The RSNA is accredited by the Accreditation Council for Continuing Medical Education (ACCME) to provide continuing medical education for physicians. The RSNA designates this journal-based activity for a maximum of 1.0 *AMA PRA Category 1 Credit*™. Physicians should claim only the credit commensurate with the extent of their participation in the activity.

Disclosure Statement

The ACCME requires that the RSNA, as an accredited provider of CME, obtain signed disclosure statements from the authors, editors, and reviewers for this activity. For this journal-based CME activity, author disclosures are listed at the end of this article. The editor and the reviewers indicated that they had no relevant relationships to disclose.

[1] From the Paul Strickland Scanner Centre, Mount Vernon Cancer Centre, Rickmansworth Road, Northwood, Middlesex HA6 2RN, England (A.R.P.); Department of Radiology, Royal Marsden Hospital, Sutton, Surrey, England (D.M.K.); and Cancer Research UK and EPSRC Cancer Imaging Centre, Institute of Cancer Research and the Royal Marsden NHS Trust, Sutton, Surrey, England (D.J.C.).
Received March 10, 2011; revision requested April 13; revision received June 9; final version accepted June 14; final review by A.R.P. August 7. **Address correspondence to** A.R.P. (e-mail: *anwar.padhani@stricklandscanner.org.uk*).

Magnetic resonance (MR) imaging plays pivotal roles in the care of patients with cancer, being used at every stage of the cancer patient's journey. While clearly important, morphologic MR imaging assessments performed with conventional sequences before and after intravenous administration of contrast material cannot be readily applied for whole-body imaging without incurring severe time penalties. Whole-body MR imaging protocols have to be tailored for each tumor type, and imaging studies can be time consuming to acquire, analyze, and report (1,2). However, there are compelling clinical and pharmaceutical needs to move toward whole-body imaging evaluations of cancer burden by using techniques that avoid radiation exposure (3).

In a recent National Cancer Institute–sponsored consensus conference report (4), it was noted that there was "an extraordinary opportunity for [diffusion-weighted MR imaging] to evolve into a clinically valuable imaging tool, potentially important for drug development." Major advantages of diffusion-weighted (DW) MR imaging include the fact that no ionizing radiation is administered and no injection of isotopes or any contrast medium is necessary. Importantly, whole-body examinations with DW MR imaging are possible in reasonably short data-acquisition times, allowing whole-body DW imaging to be incorporated into routine clinical practice (5). The information obtained can be quantified and displayed as parametric maps, thus enabling spatial heterogeneity of tissues and tumors to be analyzed before and in response to treatment. DW MR imaging–derived parameters, such as the apparent diffusion coefficient (ADC), are theoretically independent of magnetic field strength, and the relative simplicity of data acquisition facilitates multicenter and longitudinal studies (4).

In this article, we will not review in great depth what is already known about DW MR imaging, because this is already well described in many excellent reviews, scientific reports, and textbooks (4,6–8). Instead, we will focus on what we do not know about whole-body DW imaging in clinically important areas, such as histologic correlates, lesion detection, and assessment of tumor burden and therapy response. We will highlight gaps in current knowledge, gauging the relative importance of gaining new understanding to support clinical deployment and pharmaceutical trials. In so doing, we hope to stimulate research and development into this important new area of DW MR imaging applications.

Essentials

- Most modern 1.5- and 3-T MR imaging units with echo-planar and parallel imaging capabilities, high-performance gradients, and phased-array multichannel surface coils can be used to perform whole body diffusion-weighted (DW) imaging in reasonably short time intervals.
- Whole-body DW imaging may improve test performance of whole-body MR examinations because areas of increased cellularity are highlighted as high-signal-intensity regions, thus enabling "at-a-glance" assessment of normal tissues and disease burden and distribution.
- To use visual inspection of high-*b*-value images for metastasis detection, lesion characterization, and therapy assessment, it is necessary to be familiar with normal appearances of soft tissues and normal bone marrow distribution.
- Whole-body DW imaging excels at bone marrow assessment for diagnosis and for therapy evaluation, where it can potentially address unmet clinical and pharmaceutical needs for a reliable measure of tumor response.
- There are compelling needs to document and understand how treatments affect whole-body DW images and to establish response criteria, which can be tested in prospective clinical studies that incorporate measures of patient benefit.

Technical Requirements and Image Analysis

Data Acquisition

At human body temperature, thermally induced water movement in tissues is neither entirely free nor random; it is modified by interactions with cell membranes, intracellular organelles, macromolecules, and flows within tubular channels such as blood vessels and ducts. MR imaging can be used to measure water diffusivity by modifying fat-suppressed T2-weighted spin-echo sequences through incorporation of diffusion-sensitizing gradients within the measurement sequence design with the use of single-shot echo-planar readouts of the data. The strength and duration of application of diffusion-sensitizing gradients is indicated by the *b* value. In general for whole-body DW imaging, two diffusion-sensitizing gradients are used. To minimize perfusion effects, the *b* value of the lower diffusion-sensitizing gradient can be set at 50–100 sec/mm^2, resulting in "anatomic" intrinsically T2-weighted images but with vessels and cerebrospinal fluid showing marked signal attenuation; these images are often termed *black-blood images*. The higher diffusion-sensitizing gradient is typically set with *b* values between 800 and 1000 sec/mm^2; at these values, the signal intensity of many normal tissues will be attenuated to a small fraction of the initial signal intensity. Because water movement is relatively impeded in tightly packed tissues such as tumors, high-cellularity tissues appear persistently bright against an attenuated background.

Published online
10.1148/radiol.11110474 **Content codes:** GN MR

Radiology 2011; 261:700–718

Abbreviations:
DW = diffusion weighted
ADC = apparent diffusion coefficient

Potential conflicts of interest are listed at the end of this article

For the same reasons, several normal but highly cellular tissues also appear bright on high-*b*-value images, including the brain, spinal cord, normal lymphatic tissues (tonsils, adenoids, lymph nodes), and spleen (variable). For whole-body applications related to investigating cancer, it is assumed that impediments to tissue water movement are nondirectional (isotropic), so the direction of application of the diffusion-sensitizing gradients is generally unspecified or is obtained from data derived from three orthogonal DW measurements.

Recent technologic advances have enabled the development of whole-body DW imaging. Most modern 1.5- or 3-T MR imaging units with echo-planar and parallel imaging capabilities and with high-performance gradients and phased-array multichannel surface coils can be used to perform whole-body DW imaging in reasonably short time intervals. The ability to acquire very fast "snapshot" T2-weighted spin-echo echo-planar MR images by using very short echo times (<80 msec) has resulted in improved signal-to-noise ratios for DW images. Whole-body DW imaging is currently best performed at 1.5 T because of the ability to suppress fat uniformly over a large field of view. Whole-body DW imaging at 3.0 T has the potential to improve image signal-to-noise ratios but is more technologically challenging owing to the greater frequency of susceptibility artifacts and poorer fat suppression over large fields of view. Recent technologic advances, including improved shimming routines and multitransmit-equipped MR imaging systems, allow whole-body DW imaging data acquisitions at 3 T. For whole-body DW imaging applications, a multiple-averaged free-breathing data acquisition method, as originally described by Takahara et al (9), is most often used with as many stations as needed to cover the body from the top of the head to the middle of the thighs. Signal reception can use the machine's integrated body coil, but better quality images can be obtained with local surface coils. One suggested working protocol used to obtain the illustrative material in this article is provided in Appendix E1 (online).

High-*b*-value images are usually reconstructed in orthogonal planes as thin (4–5-mm) multiplanar reconstructions or maximum intensity projections (MIPs) and as thick MIPs (usually displayed in inverted gray scale). It is also possible to fuse high-*b*-value images with anatomic images by using advanced software algorithms that can aid in lesion localization. Estimates of water diffusivity on whole-body DW images (employing two diffusion-sensitizing gradients) are calculated by using monoexponential fitting to the signal decay. Voxelwise diffusivity values are displayed as parametric images, with areas of impeded diffusion appearing darker on gray-scale images. Since in vivo water movements are not free but are impeded, tissue diffusivity is often termed the *apparent diffusion coefficient* (ADC), which is reported in square micrometers per second or 10^{-3} square millimeters per second.

Qualitative Image Analysis

In patients with cancer, DW MR images should be interpreted in association with ADC maps and images obtained with conventional MR sequences, which should include examinations of the spine, abdomen and pelvis. Whole-body DW imaging may improve test performance of whole-body MR imaging examinations (10,11) because DW imaging highlights areas of increased cellularity as high-signal-intensity regions, thus enabling "at-a-glance" assessments of normal tissues and of disease burden and distribution. Initial assessments of whole-body DW images are usually made by visually assessing the signal intensity distribution on reconstructed thin multiplanar reformations and MIPs and thick MIPs from high-*b*-value images. Similar processing methods used on images obtained with lower *b* values can be also be of value. The basic biologic premise for using high-*b*-value DW images is that malignant tissues are generally more cellular and/or have higher water content than do benign and normal tissues, both of which contribute to the high signal intensities of highly cellular tissues. Visual assessments of signal intensity are clinically useful, particularly when global assessments of the tumor burden are being undertaken. This method of assessment is practically useful and clinically appealing for both radiologists and referring physicians.

In the therapy assessment setting, changes in the extent, symmetry (for bone disease), and signal intensity abnormalities can indicate the success of treatments (Fig 1). When serial studies are being compared over time, it is important to normalize the signal intensity of the thick maximum intensity projections for effective comparisons to be made. Such normalization may be undertaken by setting the window level to a tissue that is assumed to be unchanging between examinations and maintaining the window width between examinations.

Quantitative Image Analysis

There are a number of approaches for analyzing tissue ADCs, with most studies reporting median or mean values for tumor regions of interest on one or more sections (4,12–15). Whole-body DW imaging allows multiple or all lesions in the body to be evaluated together as volumes of interest. Visual inspection shows that tumors are often heterogeneous in their spatial ADC distributions, which can be evaluated with histograms. Thus, a bimodal histogram such as the one shown in Fig 1 can display different water diffusivities that reflect the cellular density distributions of tissues, which a mean or median value can never capture (16). Similarly, simple measures of central tendency have limited ability with regard to detection of treatment-related changes, particularly if there are both increases and decreases in ADCs. In these cases, the net mean or median changes in ADCs may conceal treatment-related effects (17). It is possible to capture some aspects of displayed heterogeneity in descriptors of histograms such as the range, standard deviation, centiles, skewness, kurtosis, and percentage of voxels above or below ADC cutoff values (Fig 1). Changes in histogram shape or descriptors can then be correlated with therapy response (17). Sophisticated histogram analysis approaches can also be found in the literature (18); unfortunately, these relatively

Figure 1

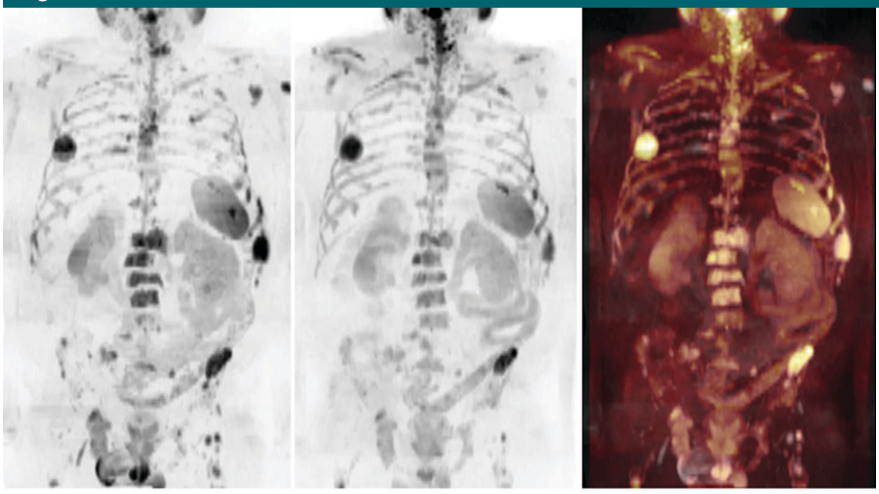

a.

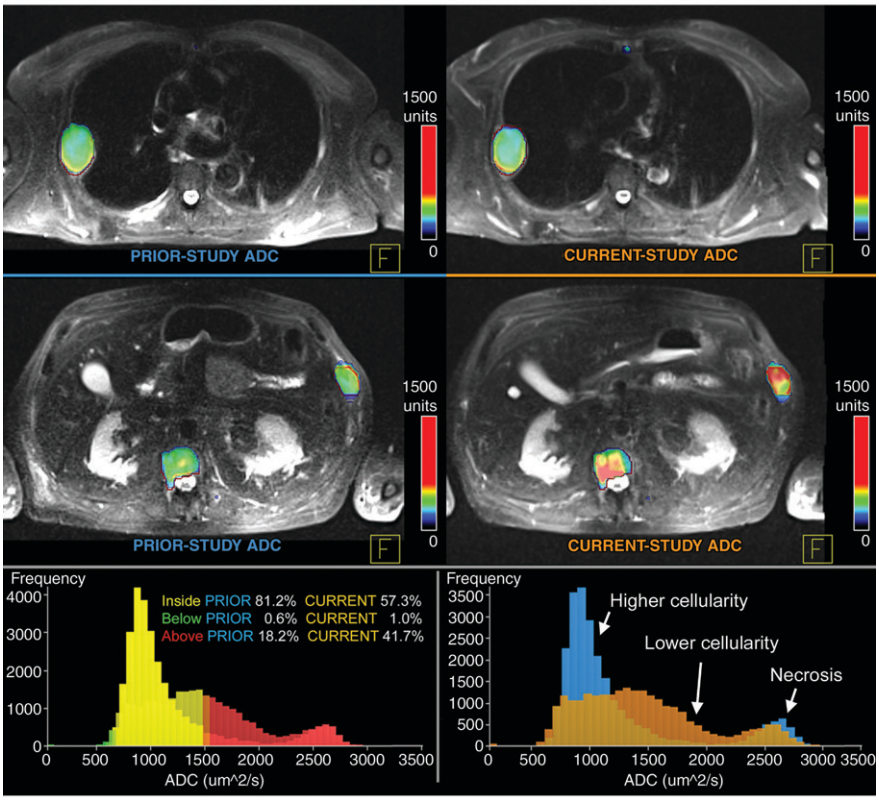

b.

Figure 1: Three-dimensional data presentation: registration and histogram analysis in a 75-year-old man with relapsed multiple myeloma before and after therapy with lenalidomide plus dexamethasone. **(a)** Inverted-gray-scale whole-body DW MR images (b = 900 sec/mm^2) obtained before therapy (left) and after 7 months of treatment (middle) and software-enabled fusion of the pre- and posttherapy (right). Mixed response to therapy is seen, with signal intensity reductions in many lesions (spine, pelvic bone marrow) but persistent hyperintensity of right fourth rib and of lesion in the anterior left iliac crest. **(b)** Fusion images from short tau inversion-recovery MR imaging and ADC map of right rib region of interest show no change in ADC (pretherapy, 874 μm^2/sec; posttherapy, 834 μm^2/sec) (top row) but increases in ADC of spinal (pretherapy, 887 μm^2/sec; posttherapy, 1215 μm^2/sec) and left ninth rib lesions (pretherapy, 986 μm^2/sec; posttherapy, 1433 μm^2/sec) (middle row). Bottom right: Histograms before (blue) and after (orange) therapy were obtained by using whole-body tumor regions of interest defined on pretherapy images applied to posttherapy volume after image registration. Pretherapy bimodal histogram changes to trimodal histogram (mean pretherapy *[PRIOR]* ADC, 1010 μm^2/sec $\pm$ 573; ADC, 1366 μm^2/sec $\pm$ 562). Bottom left: Segmented histogram with thresholds at 1500 and 2500 μm^2/sec confirm increasing percentage of voxels with higher ADCs after therapy *(CURRENT)* consistent with reductions in cellularity after therapy.

complex approaches tend to remove them from clinical usability because of uncertainty about their biologic meaning. A major disadvantage of the histogram approach is that the spatial distribution of ADC information can be lost.

A recently introduced analytic method for retaining spatial information in response to therapy is called the *functional diffusion map* or the *ADC parametric response map* (19). This method requires that pre- and posttherapy ADC volumes are spatially registered by using sophisticated software. Differences in the registered voxel data between the two data sets are determined, and threshold values for ADC change are applied according to predetermined criteria. Changes in voxels are then color labeled and overlaid on anatomic images, enabling the spatial distribution of changed voxels to be appreciated. This approach also allows the quantification of the relative tumor volume in which changes have occurred. The method appears to work reasonably well for studies of the brain and for some bone regions (20) but appears less suited for tumors located in areas of the body with substantial physiologic motion (eg, thorax and abdomen) and for organs with considerable tissue and tumor distortions. The technique also requires images with a high signal-to-noise ratio, because image noise can lead to substantial

variation of ADCs at the voxel-by-voxel level, thus confounding interpretations. In addition, the technique cannot be easily applied when there are observable changes in tumor size or shape after treatment. Furthermore, thresholds of individual voxel differences need to be prospectively defined to ascertain the percentage of voxels that are changed in response to a therapeutic intervention; these thresholds are yet to be defined in the various organs where the method is applicable.

An important consideration when assessing ADC changes in response to therapy is whether to adjust the volume-of-interest sizes according to volume changes that occur in response to therapy. It is attractive to retain region-of-interest definitions if one can be assured that effective image registration has been performed between the examinations in question. As previously noted, this method is particularly applicable when evaluating lesions in the bone marrow and brain. With regard to its use for evaluating bone lesions, this method of analysis could be helpful when evaluating metastases that apparently "disappear" on high-*b*-value DW images either because the signal intensity of the metastasis becomes reduced to that of normal background levels or when therapy-induced bone marrow hyperplasia (which effectively increases background signal intensities) is present. On the other hand, ROI definitions should be adjusted to size changes for soft tissues (because robust registration cannot always be ensured) and for bone metastases that progress with therapy. Volume-of-interest adjustment is also required when there is a need to evaluate tumor volumetric response to therapy (Fig 2). Volume-of-interest definitions and their clinical use are important new research areas. Further research and development perspectives regarding data acquisition and display methods are listed in Table 1.

Normal Appearances

To use visual inspection of high-*b*-value images for metastasis detection, lesion characterization, and therapy assessment, it is necessary to be familiar with the normal appearances of soft tissues and the normal distribution of bone marrow and to correlate DW imaging findings with those obtained with morphologic imaging sequences. Review of the literature shows that there is incomplete documentation of what constitutes normality on DW MR images in the various anatomic regions. Our experience suggests that normal signal intensity appearances need to take into account both hyperintense areas and hypointense areas (Table 2). This is particularly true when assessing bone marrow, because bone metastases are a common disease manifestation in oncology. With regard to visual inspection, whole-body DW images are excellent at demonstrating the variability of normal bone marrow distribution. Readers should recall that the normal adult bone marrow distribution becomes established by 25 years of age and that yellow bone marrow has low water content (10%–20%) (21–23), which results in decreased signal intensity on DW images. On the other hand, red bone marrow has increased cellularity and water content (40%–60%) (23,24), thus resulting in higher signal intensity on DW images. There are variable amounts of red bone marrow atrophy and trabecular bone loss after 40 years of age (25), particularly in women (possibly related to estrogen deficiency and osteoporosis [26]), resulting in increased adiposity, which thus lowers the signal intensity of bone marrow on whole-body DW images as age increases.

Variations in the cellularity of bone marrow affect the signal intensity of bones on high-*b*-value images. One of the most common causes of a reduction in the signal intensity of normal bone marrow is cytotoxic chemotherapy, which causes modest fatty bone marrow atrophy (Fig 2). However, the extent, timing, and direction of change in normal bone marrow on DW MR images in response to chemotherapy have not been established. Another area of potential difficulty in the assessment of bone marrow is the effect of growth factors such as granulocyte colony stimulating factor (G-CSF). G-CSF administration during chemotherapy (for moderation of neutropenic complications during treatment) results in increased signal intensity on whole-body DW images that can mimic disease progression (Fig 3) (27). This is due to increased bone marrow cellularity and water content. The effects on bone marrow signal intensity can occur within 2 weeks of the first G-CSF dose (28), but it is unclear whether additional doses further alter bone marrow signal intensity or there is resolution of changes on cessation of therapy. It is, therefore, potentially challenging to differentiate between new pathologic bone marrow infiltrations and benign red marrow reconversion changes related to G-CSF. Furthermore, bone metastases can become less conspicuous with increasing bone marrow signal intensity that has been caused by G-CSF, which makes therapy assessment more difficult. The effects on whole-body DW imaging of bone marrow of other commonly used hematopoietic growth factors (erythropoietin and granulocyte macrophage colony stimulating factor) remains largely undefined. Other causes of bone marrow hypercellularity and hypocellularity commonly observed in cancer patients are listed in Table 3.

There are a number of potential confounding factors that demonstrate high signal intensity on high-*b*-value images (leading to false-positive interpretations) such as tissue edema and inflammation after radiation therapy or surgery. Increased lesion or tissue signal intensity, relative to background signal intensity, on high-*b*-value images (with corresponding increased ADCs) can result from increased water content and is termed *T2 shine through*. The T2 shine-though effect can be reduced by increasing the strength of *b* value gradients but at the expense of increasing image noise. Alternative sources of increased signal intensity also include long T1 relaxation times and high proton density; tissue T1 is a substantial source of contrast when inversion-recovery techniques are used for fat suppression. T2 shine through is responsible for the visibility of normal salivary and prostate glands, gall bladder, liver hemangiomas, and occasionally normal breast parenchyma on whole-body

Figure 2

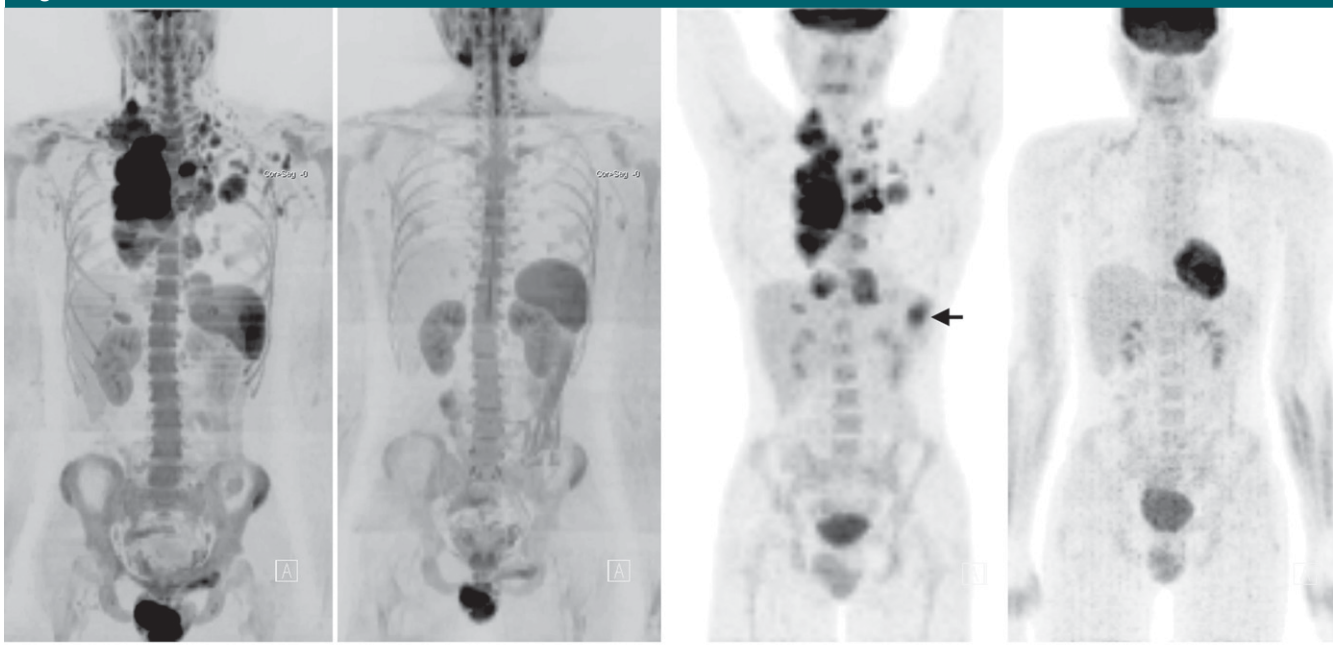

a. b.

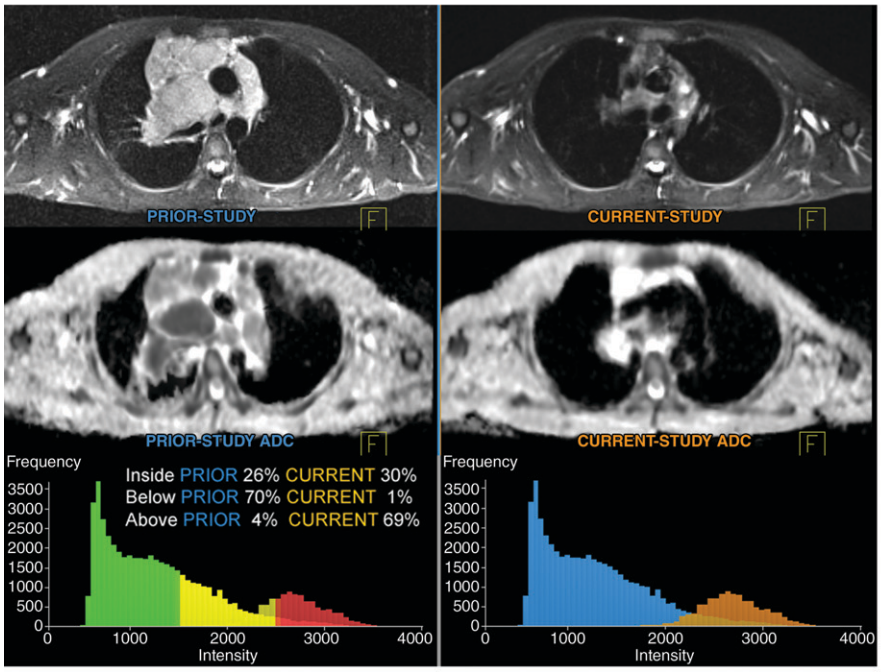

c.

Figure 2: Whole-body DW imaging versus fluorine 18 (^{18}F) fluorodeoxyglucose (FDG) positron emission tomography (PET) for monitoring therapy response in a 23-year-old man with Hodgkin lymphoma treated with doxorubicin-bleomycin-vinblastine-dacarbazine chemotherapy. **(a)** Inverted-gray-scale DW images (b = 900 sec/mm^2) obtained before (left) and 5 months after treatment (right) show supradiaphragmatic distribution of nodal disease. Splenic signal intensity is considered to be within normal limits. There is some variation in signal intensity of the top station, compared with that of middle and lower stations, of DW images. Bone marrow signal is hyperintense but normal for age. Note that glans penis is projected over the left superior pubic ramus. After therapy, no hyperintense signal is seen at sites of nodal disease, consistent with therapy response. Note interval development of bone marrow hypointensity (both pre- and posttherapy DW images are normalized to right kidney signal intensity). **(b)** Whole-body FDG PET scans obtained before (left) and after therapy (right) show complete response to therapy. FDG PET scan shows splenic deposit before therapy (arrow), which is not visible on **a. (c)** Axial short tau inversion-recovery MR images (top row) and ADC maps (middle row) through mediastinum show reductions in nodal tumor volume (pretherapy, 703 cm^3; posttherapy, 166 cm^3) and marked increases in ADC. Histograms before (bottom right: blue) and after (bottom right: orange) therapy were calculated by using regions of interest adjusted to visible volume of nodal disease. After therapy, there are few voxels in the histogram because of reductions in tumor volume; marked increases in ADC are seen (pretreatment mean,1180 μm^2/sec $\pm$ 550; posttreatment mean, 2550 μm^2/sec $\pm$ 380). Segmented histograms (bottom left) with thresholds at 1500 and 2500 μm^2/sec confirm increasing percentage of voxels at higher ADC values after therapy *(CURRENT),* consistent with reductions in cellularity, compared with pretherapy *(PRIOR)* values.

Table 1

Research and Development Needs for DW Imaging Data Acquisition, Display, and Analysis

Method	Requirements
Image quality	Developmental efforts to ensure that high-quality images can be acquired for both qualitative and quantitative assessments across MR platforms to allow meaningful comparison of results from different imaging centers*
ADC estimates	Increase accuracy of ADC estimates: Currently used two-point monoexponential fitting of *b* values may lead to erroneous ADC estimates, particularly if the higher *b* values are at the noise floor for a particular tissue†
Signal intensity normalization	Normalization of signal intensity between imaging stations in a particular examination and for comparing whole-body maximum intensity projections acquired serially over time are needed to enable evaluations of changes*
Automatic segmentation	Improve ability to automatically segment DW images to derive tumor volumes (for discrete and diffuse infiltrations) and to obtain whole-body tumor ADC histograms†
Volume of interest definition	Investigate best methods for defining volumes on whole-body DW images (eg, anatomically defined, from high-*b*-value images, ADC maps, or combinations thereof) before and during therapy to minimize observer variability in ADC and tumor volume estimates†
Image registration	Improve ability to register multiple whole-body DW images to enable comparison of whole-body and regional changes in tumor volume and ADCs in response to therapy‡
ADC parametric response mapping	Investigate anatomic applicability and thresholds for ADC parametric response mapping to assess clinical value of this approach‡

Note.—Authors' subjective assessments of research needs.

*Definite requirement for clinical deployment & drug development.

†Could be clinically important.

‡Absence of knowledge unlikely to hinder technique deployment.

Table 2

Normal Appearances on Whole-Body DW MR Images

Tissue	Appearance*
Brain, spinal cord, nerve plexuses, ganglia	Hyperintense
Normal lymph nodes and spleen (highly variable)	Hyperintense
Adrenal and salivary glands	Hyperintense
Bowel mucosa and contents	Hyperintense
Penis, testes, ovaries, normal endometrium and prostate gland	Hyperintense
Normal red bone marrow	Hyperintense
Breast tissue, according to menstrual cycle	Hyperintense
Sluggish flow in veins (occasionally)	Hyperintense
Mediastinum, left lobe of liver, heart, near diaphragm (incoherent motion)	Hypointense
Lung (low water content)	Hypointense
Normal yellow bone marrow	Hypointense

*Hyperintensity is due to long T2 relaxation times, impeded water movement, or both.

DW images (Table 2). To prevent misinterpretations due to signal intensity assessments, it is necessary to correlate high-*b*-value images with corresponding ADC values by using the interpretation guidelines given in Table 4, also taking into account morphologic features on images obtained with other MR sequences.

The following are further research and development perspectives regarding normal appearances:

1. Full documentation of the normal appearances in the various anatomic regions is needed. This includes the appearance of the cycling endometrium, elucidation of the causes of the variable signal intensity appearances of the spleen, and documentation of lymph node size and distribution at various anatomic locations. Absence of such knowledge is unlikely to hinder technique deployment.

2. An atlas of signal intensities and ADCs of the normal bone marrow distribution through the age decades and factors that affect appearances (eg, sex, race, fat-to-water ratio) need to be developed to improve the detection of pathologic bone infiltrations and for assessment of therapy response. This information is a definite requirement for clinical deployment and drug development.

3. Documentation of the appearances of normal and benign conditions that may mimic pathologic bone infiltrations (eg, age-related arthritis, spinal and liver hemangiomas, nerve ganglia) could be clinically important.

Histologic Correlates

The high signal intensities observed on high-*b*-value images and lower ADCs of malignant tissues can be attributed to the fact that malignant tissues are generally more cellular and/or have higher water and protein content than do benign and normal tissues (29,30). There are a number of microscopic organizational features that can also affect the water diffusivity of tissues, including microperfusion, cell density (number of cells per high-power field), cell nuclear-to-cytoplasm ratio, integrity of cellular membranes, distribution of cell sizes within a tissue, and tortuosity of the extracellular space–cytoarchitectural tissue organization.

Inverse correlations between ADC and cell density have been shown repeatedly in gliomas, metastatic brain tumors and renal, breast, and prostate cancers, as well as in some childhood tumors (31–41). ADC correlations in bone marrow as a consequence of disease

Figure 3

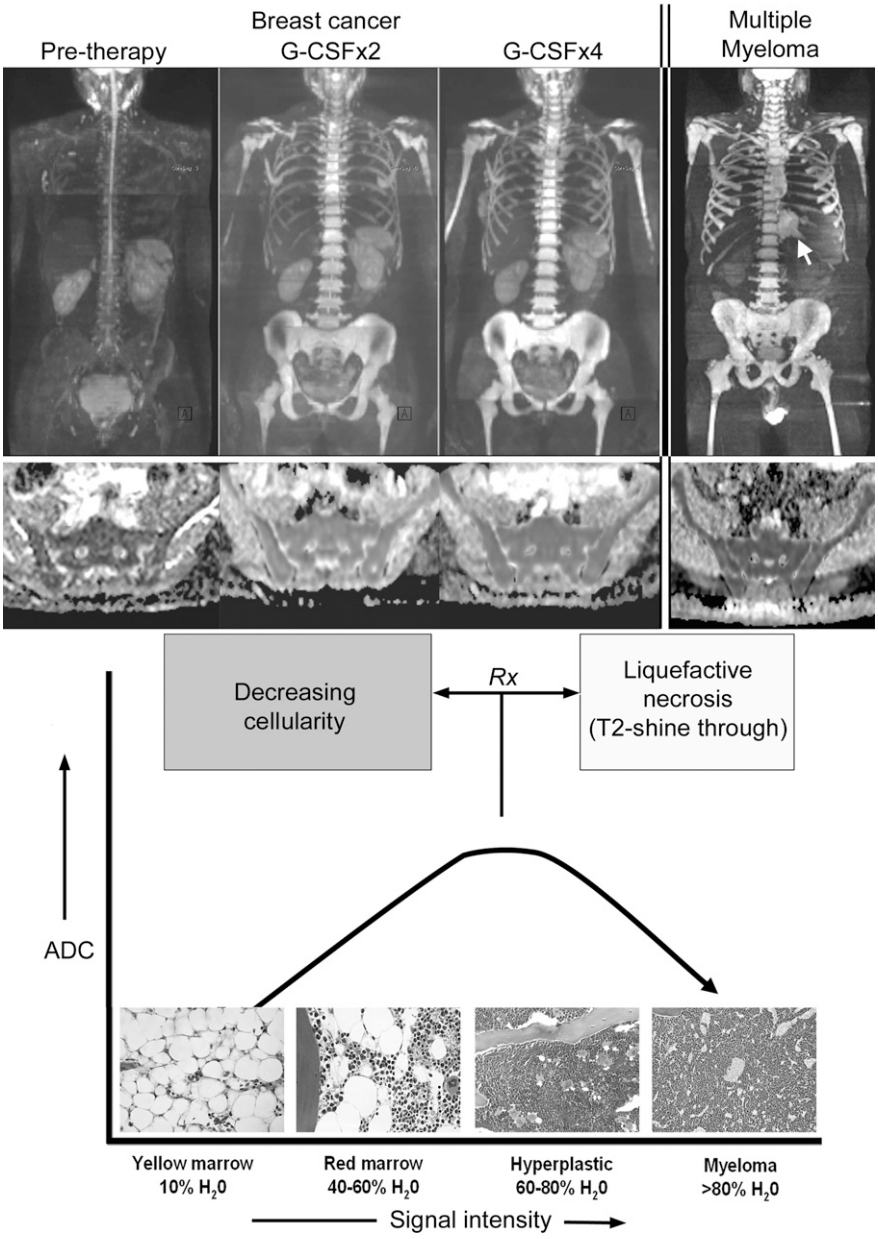

Figure 3: Possible relationship between bone marrow cellularity and water content on DW MR images in a 51-year-old woman who had undergone left breast mastectomy and left axillary node dissection and in a 54-year-old man with multiple myeloma. Top: whole-body DW images. Top, three leftmost images: Pretherapy images (original gray scale) show low signal intensity and low ADC caused by abundance of fatty cells and low water content. ADC of sacrum is 800 μm^2/sec $\pm$ 216. After two cycles of granulocyte colony stimulating factor *(G-CSFx2)* administration to support taxane chemotherapy, bone marrow cellularity increases due to replacement of fat cells and increases in water content, leading to increases in signal intensity and ADCs. ADC of sacrum now is 990 μm^2/sec $\pm$ 65. After four cycles *(G-CSFx4),* further increases in signal intensity of humeral diaphyses are seen, but ADCs have decreased slightly. ADC of sacrum is 920 μm^2/sec $\pm$ 60. Top right image: Homogeneous infiltrating bone marrow pattern and a paraspinal plasmacytoma (arrow) are shown. Patient had presented with pancytopenia. Low signal intensity of the spleen is due to transfusion hemosiderosis. Increased bone marrow cell density causes reduction in ADC of the sacrum (710 μm^2/sec $\pm$ 85). (All whole-body DW images were normalized to right kidney signal intensity to enable comparisons among sequential DW images.) Bottom: Schematic representation of relationship among cellularity, signal intensity, ADC, and water content, with histologic examples. Successful therapy *(Rx)* would result in increased ADCs and decreased signal intensity consistent with decreasing cellularity, but T2 shine-through effects after therapy would increase both signal intensity and ADC.

merit separate consideration. Our observations, supported by the literature, suggest that ADC correlations with cellularity of the bone marrow are noninverse, but the explanation for this phenomenon is incompletely understood (42–45) (Fig 3). On whole-body DW images, yellow fatty marrow is of lower signal intensity and has lower ADC (13), probably because of the reduced proton density of yellow marrow, the hydrophobic nature of fat, and lower bone marrow perfusion (compared with red bone marrow) (46). With increasing bone marrow cellularity (which displaces fat cells and increases vascularization of the bone marrow), the signal intensity on high-*b*-value images increases and appears to paradoxically return higher ADCs compared with yellow bone marrow (13,44,45,47,48). Once all fat cells are lost, however, increasing bone marrow cell density may then cause some ADC reductions (as in non–bone marrow tissues [31–41]), but this effect has not been comprehensively documented.

There are other important histologic properties that correlate with ADC, including tumor proliferation index (41,49,50), tumor grade (51–56), presence of necrosis (37,57–60), and, in the therapy setting, tumor cell apoptosis (57,61,62). Thus, low ADCs in tumors have been correlated with histologic features indicative of poor prognosis such as tumor grade (55,63) in prostate and breast cancers and vascular invasion in breast cancer (63), as well as with other markers of poor prognosis such as tumor size (52,64) and nodal

Table 3

Common Causes and Diffuse Effects on Bone Marrow Cellularity That Affect DW MR imaging Signal Intensity in Cancer Patients

Cause	Effect
Radiation changes (whole body radiation exposure or localized bone radiation)	Hypocellularity resulting in lower signal intensity
Neoplastic disorders of bone marrow (myelodysplasia and myelodysplastic syndrome, primary myelofibrosis and myeloid metaplasia)	Hypocellularity resulting in lower signal intensity
Marrow disorders: aplastic anemia (primary autoimmune; secondary: metal poisoning [gold-, arsenic-containing compounds], drugs [including alcohol], viral infections [hepatitis, Epstein-Barr virus], chronic infection [tuberculosis]), and myelofibrosis	Hypocellularity resulting in lower signal intensity
Drugs: cytotoxic chemotherapy and myelotoxic drugs, radiomimetic drug administration and toxicity	Hypocellularity resulting in lower signal intensity
Poor nutrition; iron, folate, and vitamin B_{12} deficiencies	Hypocellularity resulting in lower signal intensity
Chronic disease (renal failure, chronic liver disease, rheumatoid disease)	Hypocellularity resulting in lower signal intensity
Older age and osteoporosis (including postmenopausal and drug induced)	Hypocellularity resulting in lower signal intensity
Prolonged immobility	Hypocellularity resulting in lower signal intensity
Children and young adults	Hypercellularity resulting in higher signal intensity
Chronic anemia	Hypercellularity resulting in higher signal intensity
Living at high altitude and athletes	Hypercellularity resulting in higher signal intensity
Smoking	Hypercellularity resulting in higher signal intensity
Chronic cardiac failure	Hypercellularity resulting in higher signal intensity
Pregnancy or recent pregnancy	Hypercellularity resulting in higher signal intensity
Hematopoietic growth factors therapies, including granulocyte-colony stimulating factor	Hypercellularity resulting in higher signal intensity

Table 4

Image Interpretation Guidelines for DW MR Imaging

Signal Intensity*	ADC Maps	Interpretation
High	Low	Generally, high-cellularity tumor; rarely abscess, viscous fluids, or blood products
High	High	T2 shine through; liquefactive necrosis
Low	High	Fluid; necrosis; lower cellularity; occasionally well-differentiated adenocarcinomas
Low	Low	Fibromuscular tissues, fat, susceptibility artifact
Low	Low or intermediate	Mature fibrous tissue with low water content

*On high-*b*-value DW images.

metastases (63–65). Lower tumor ADCs also place patients into clinical groups with poor prognosis, according to the D'Amico classification for prostate cancer (55) and the Nottingham prognostic index for breast cancer (63).

As a result, it has now been found that ADCs can also be used to determine the likelihood of a tumor responding to treatment. For example, a high ADC before treatment has been shown to predict an unfavorable treatment response in preclinical and clinical studies (66–69), probably because a high ADC reflects the presence of tumor necrosis and low oxygen tensions. Tumor hypoxia is known to mediate resistance to chemotherapy, radiation therapy, and photodynamic therapy, leading to the selection of aggressive tumor cell clones capable of evading the hostile tumor microenvironment (70,71). However, the association between high ADC and less favorable response to treatments does not apply to all therapy types (72). Indeed, the opposite has been found for vascular disruptive agents, which are known to induce massive central necrosis in tumors. The results from early preclinical (73,74) and clinical studies (14) indicate that higher pretreatment ADCs were more susceptible to the effects of the vascular disruptive agent combretastatin A4 phosphate.

We believe that further research and development perspectives regarding normal bone marrow and its response to systemic therapies are needed, as follows:

1. The relationship between DW imaging findings (signal intensity and ADC) and bone marrow cell density requires mechanistic clarification in terms of the relative influences of bone marrow cell type, cellular density, fat content and type, water, and trabecular bone density. This is a definite requirement for clinical deployment and drug development.

2. There is limited documentation on how common treatments such as chemotherapy and hormonal therapy affect the signal intensity of normal bone marrow. Such information could be clinically important.

3. Knowledge is scarce regarding how novel antiproliferative and noninvasive therapies affect normal appearances on whole-body DW images; this is important because these therapies can be myelotoxic and thus affect bone marrow cellularity and bone scan appearances. Further knowledge is a definite requirement for clinical deployment and drug development.

4. There is minimal documentation on the effects of hematopoietic growth factors (erythropoietin, granulocyte colony-stimulating factor, granulocyte macrophage colony-stimulating factor) on whole-body DW imaging results in terms of the timeline of changes and the extent and direction or potential reversibility of changes. More information is a definite requirement for clinical deployment and drug development.

5. There is minimal knowledge regarding how treatments that target bone trabeculae, such as bisphosphonates and denosumab, affect the signal intensity on whole-body DW images. Further knowledge could be clinically important.

Lesion Detection and Characterization

Whole-body DW imaging is an attractive lesion detection technique because it enables "at-a-glance" assessments, where one's attention is immediately drawn to potential abnormal regions, which helps reduce the image interpretation times of anatomic whole-body MR imaging (5). Whole-body DW imaging can be considered a supplement to anatomic whole-body MR imaging, leading to improved reader performance of the latter (75). The capability of whole-body DW imaging to improve sensitivity for detection of bone metastases is at the expense of specificity, as was illustrated in a recent meta-analysis (76).

Lesion Detection

The ability to detect lesions on whole-body DW images is highly dependent on tumor histologic type and grade, as well as on anatomic location. Thus, in our experience, detection ability is good for breast cancers, myeloma, and lymphoma and for tumors with tightly packed small cancer cells such as neuroendocrine tumors, small cell cancers, and many childhood tumors (13,77–80). Metastatic diseases from these tumor types generally appear bright on high-*b*-value images. In contradistinction, primary tumors and metastases from renal cancers are sometimes less well seen, with clear cell metastases appearing relatively less conspicuous compared with other renal cancer histologic subtypes (papillary or chromophobe); this may be related to the relatively greater water diffusivity in clear cell cancers (31,54, 81,82). Furthermore, it has been noted that well-differentiated or low-grade masses are less well seen, probably because they often have a more normal-appearing histomorphologic structure (52–56,83). The latter point is not a hard and fast rule, because many cytologic features other than cellular density determine tumor grade.

There are several anatomic "blind spots" where lesion detection is impaired (leading to false-negative results), including the mediastinum, at the pulmonary hila, and in the most cranial aspect of the left hepatic lobe, just beneath the heart. At these sites, complex incoherent motion contributes to decreased signal intensity on high-*b*-value images. Motion-related signal intensity decreases may explain why metastatic lesions in the bone marrow of the anterior chest wall are sometimes relatively less conspicuous than lesions found in the spine and paraspinal regions. Last, small lung metastases are poorly depicted on whole-body DW images, although a sensitivity analysis by lesion size has not been performed, to our knowledge.

On the other hand, whole-body DW imaging excels at lesion depiction in the bone marrow; it is better than computed tomography (CT) and bone scans for demonstration of bone disease (13,84) (Fig 4). Causes of false-positive increases in bone marrow signal intensity on DW images include bone marrow edema caused by fracture, degenerative disease, bone infarction, infection, and hemangioma. Other causes of false-positive focal increases in signal intensity on DW images include isolated islands of red bone marrow within yellow marrow and treated, but inactive, lesions (T2 shine through). Many of these false-positive increases in signal intensity on high-*b*-value images can be overcome by performing image interpretations with ADC maps and conventional images. Causes of false-negative results in bone marrow tumor detection include low levels of tumor infiltration, skull vault and skull base metastases (due to adjacent high signal intensity of the brain), and metastases that develop within hypercellular bone marrow. As a general rule, lytic bone metastases are better seen than sclerotic and treated lesions because of the lower water and cellular content (13,85). The latter may not be a substantial disadvantage for whole-body DW imaging in the response-assessment setting, because many treatments for osteolytic disease, including bisphosphonates, zelodronic acid, and denosumab, reduce the frequency of adverse skeletal-related events by inhibiting osteoclastic action, thus converting osteolytic to sclerotic lesions. In this regard, readers should remember that osteolytic disease is frequently associated with bone pain, the effects of hypercalcemia, pathologic fractures, and spinal cord compression. Indeed, an osteoblastic reaction detected on CT scans is a recognized response criterion when there are other signs of response (86).

Lesion Characterization

The ability of whole-body DW imaging to characterize soft-tissue lesions is more limited when signal intensity information alone is used for assessments, without regard to morphologic appearance and ADC. We have already noted that this is due to the fact that signal intensity on high-*b*-value DW MR images is related to long T2 relaxation times and/or impeded water movement. It is only when signal intensity information is combined with ADCs that DW MR imaging findings are able to serve as a biomarker of cellularity, which can then be used with anatomic knowledge for tissue characterization by using the guidance listed in Table 4 (12,41,55,87).

Lymph node assessments are most commonly evaluated by using size criteria on DW MR images (88), but nodal size is known to be relatively poor for discrimination between benign and malignant nodal disease. DW MR imaging has limited abilities with regard to characterization of lymph nodes for involvement by metastatic disease, because *(a)* there is an overlap in ADCs of benign and malignant nodes, *(b)* the inconsistency of ADC cutoff values among different studies, and *(c)* high observer variability

Figure 4

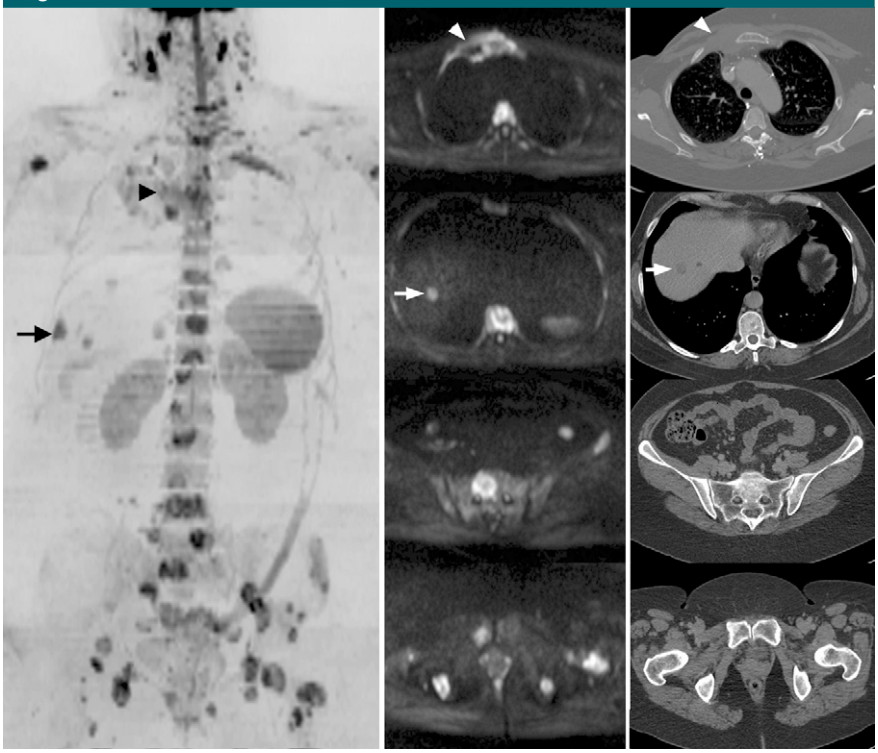

Figure 4: Whole-body DW imaging versus CT for detection of bone metastases in 51-year-old woman with metastatic breast cancer and history of right mastectomy and axillary nodal dissection. Extensive bone metastases are well depicted on whole-body DW (left; inverted gray scale) and source DW (middle; original gray scale) images. Bone metastases are poorly depicted on corresponding unenhanced CT scans (right) obtained 2 weeks later (bone and soft-tissue windows at various levels). Arrowhead = parasternal recurrence, arrow = liver metastasis.

in defining regions of interest for measurement of ADCs of small lymph nodes (89–99). There is growing evidence that lymph node ADCs do provide some discriminatory value (89–99). For example, Lin et al (89) evaluated patients with endometrial or cervical cancer and found that ADCs were significantly lower for malignant than for benign nodes (600 vs 2100 μm^2/sec; $P < .001$). Using a cutoff of 1000 μm^2/sec, they found that the combination of nodal size and relative ADC demonstrated a significant improvement in sensitivity for metastatic disease, from 25% to 83%, while specificity remained high at 99% and 98% (89). Kim et al (100) also found significantly lower ADCs in malignant nodes than in nonmalignant nodes (765 μm^2/sec ± 114 vs 1002 μm^2/sec ± 186; $P < .001$) in patients with cervical cancer. The sensitivity and specificity of ADC for differentiation of metastatic from nonmetastatic lymph nodes were 87% and 80%, respectively. However, two studies (101,102) did not demonstrate an improvement in the characterization of nodal disease. The combination of whole-body DW imaging and ultrasmall superparamagnetic iron oxide contrast agents may improve diagnostic performance of DW imaging for discrimination of malignant from benign nodes (103); investigations into this important new way forward have been hampered by the current nonavailability of the contrast agent.

Comparisons of Whole-Body DW Imaging and FDG PET for Lesion Detection and Characterization

^{18}F fluorodeoxyglucose (FDG) PET and whole-body DW imaging should be regarded as complementary techniques in the assessment of cancer patients, because they interrogate completely different biophysical tissue properties (glucose metabolism vs cellular density). Inverse correlations between specific uptake value at PET and ADC have been noted in some reports (63,104,105). In practice, it has been noted that FDG PET can be used to successfully evaluate anatomic regions where whole-body DW imaging is often nondiagnostic, such as lymph nodes, mediastinal structures, lungs, and spleen (Fig 2). On the other hand, whole-body DW imaging is of value when evaluating anatomic regions where high levels of FDG accumulate, such as the brain, renal collecting system, and urinary bladder. Whole-body DW imaging is also helpful for the evaluation of cancers associated with low levels of FDG uptake, such as prostate cancer, neuroendocrine tumors, hepatomas, thyroid cancers, and certain types of low-grade lymphomas (106), or when the metabolic dimensions are too small to be confidently resolved on PET images. The recent introduction of hybrid PET/MR imaging systems will encourage investigations into the added value of combining PET and whole-body DW imaging information for lesion detection and characterization and assessment of therapy response (107).

Research and development perspectives.—Further research and development perspectives regarding lesion detection and characterization are as follows:

1. Investigations of the differences in ADCs between benign and malignant nodes for the entire range of malignant diseases are required. It may be that the success of ADC nodal measurements is dependent on histologic subtype, including the relative incidence of microscopic to macroscopic disease. These investigations are a definite requirement for clinical deployment and drug development.

2. Documentation of observer variability of nodal ADC measurements (including size dependence) is required and needs to be considered when evaluating the utility of ADC measurements to distinguish malignant and benign nodes. Such documentation could be clinically important.

3. Do tumor volume estimates on whole-body DW images or ADC histograms correlate with biomarkers of tumor load such as serum tumor markers, circulating tumor cells, and tumor DNA? Do DW MR imaging biomarkers correlate with other markers of changing tumor burden and cell death in therapy assessment settings? Answers to these questions could be clinically important.

4. Comparison of whole-body DW imaging with other whole body imaging techniques such as CT, conventional MR imaging, PET (with its varieties of tracers), and bone scintigraphy for lesion detection are required. This could be clinically important.

Treatment Response

As a general rule, any pharmacologic, physical, or radioactive process that causes necrosis or cellular lysis will lead to an increase in water diffusion in the extracellular space, with decreases in signal intensity on high-*b*-value images and corresponding increases in ADCs (8,108–110) (Figs 1, 2). On the other hand, disease progression is displayed as new areas of abnormal signal intensity or as increases in the extent and intensity of previously documented abnormalities (Fig 5). Because cellular death in response to treatment precedes changes in lesion size, changes in DW MR imaging findings may be an effective early marker of response for therapies that kill tumor cells. Increases in ADC accompanying tumor cell death may not persist, and ADC does decline subsequently as dead cells are removed by tissue macrophages, tissues become remodeled, the vasculature normalizes, and mature fibrosis develops (111). Of course, if tumors become resistant to therapy, that, too, may decrease ADC—a potential pitfall.

Soft-Tissue Response

Increases in ADC after successful chemotherapy and radiation therapy have been noted in several anatomic sites, including breast cancers (112,113), primary and metastatic liver cancers (68, 114,115), primary bone sarcomas (60, 116–118), and brain malignancies (119, 120). In soft-tissue sarcomas treated with chemotherapy, increases in ADC are associated with reduction in tumor size and vice versa; as a result, strong negative correlations between tumor volume and ADC changes have been reported (r =-0.925, $P < .0001$) (121).

Studies of both animal tumors (122,123) and some human cancers have shown that increases in ADC can occur rapidly after the first dose of chemotherapy (Fig 2). A recent study (68) in human patients examined the onset of changes in ADC in liver metastases from stomach and colorectal cancer; ADC increases were noted as early as 3–7 days after the first dose of chemotherapy and ADC increases were also seen to correlate with therapy response. Theilmann et al (114) evaluated 60 liver metastases before and after chemotherapy in 13 women with breast cancer. Increases in ADC were observed 4–11 days after the start of therapy, particularly in smaller lesions. A number of studies have evaluated ADC changes in patients with primary breast cancer treated with neoadjuvant chemotherapy. Stepwise increases in ADCs were shown with each therapy cycle in responding patients, with changes in diffusivity preceding changes in tumor size or volume (112,124).

A number of preclinical and clinical studies have used DW MR imaging to evaluate the effects of external-beam radiation therapy. Preclinical studies show that ADC increases occur rapidly in tumors that are radiation sensitive (125), with changes visible as early as 24–72 hours after a single large radiation fraction (126). This finding occurred in the absence of a change in tumor size and coincided with metabolic disruption shown with proton MR spectroscopy (126). Such increases in ADC were not seen in squamous cell cancers that were

Figure 5

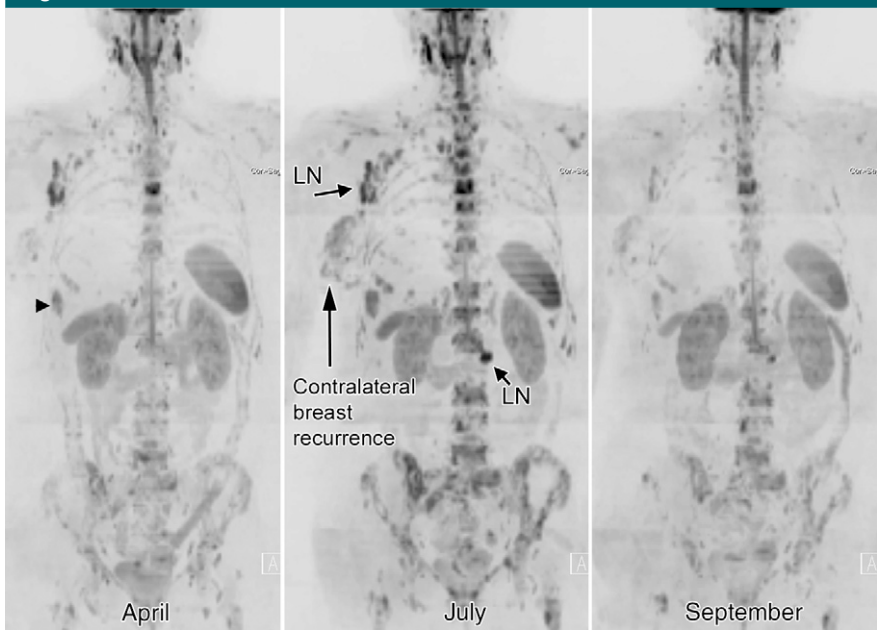

Figure 5: Modification of therapy on the basis of whole-body DW imaging findings in a 45-year-old woman with metastatic breast cancer and history of left mastectomy and axillary nodal clearance. Left: Baseline image obtained in April shows widespread bone metastases, right-sided axillary nodal enlargement, and liver metastases (arrowhead) (confirmed on axial images). Middle: First follow-up image (obtained in July) after 3 months of therapy with herceptin, anastrozole, and bisphosphonate shows disease progression in bones, right axillary and upper abdominal lymph nodes *(LN)* (short arrows), contralateral right breast (long arrow) and liver. Treatment was changed to gemcitabine and carboplatin chemotherapy. Right: Second follow-up image (obtained in September) shows responding disease at all disease sites.

radiation resistant unless concomitant chemotherapy was administered (127). Increases in ADC appear to occur incrementally in fractionated regimens, with the greatest increases visible at the end of therapy (111). Increases in ADC are likely to be related to tumor cell death, the development of tissue edema due to inflammation, and increased microvessel leakiness.

In patients with malignant liver lesions, increases in ADC have also been seen 7–14 days after the start of external-beam radiation therapy, with greater increases correlating with higher doses (128). Early increases in ADC (1–3 weeks) have also been noted for squamous cell head and neck cancers, brain gliomas, locally advanced rectal cancer, and uterine cervical cancers treated with combination chemotherapy and radiation therapy (69,129–133). In fact, a number of clinical studies have shown that the failure to increase tumor ADC in response to radiation or combined chemo- and radiation therapy results in a poorer response to therapy (119,128,130,134).

Bone Marrow Response

When bone marrow disease is treated successfully, then tumor cell death results in decreases in signal intensity on high-*b*-value images and increased ADC. This has been shown in patients with leukemia, who had marked increases in ADC that correlated with successful treatment (135). DW MR imaging to monitor treatment response of vertebral metastatic deposits also showed convincing changes from hyperintensity to hypointensity on high-*b*-value images after chemotherapy in patients with clinical improvement (136). T1-weighted and T2-weighted spin-echo MR images of spinal metastases often reveal no substantial interval changes, which indicates that these MR sequences were of limited use for monitoring response to therapy (136). Equally, patients with no clinical improvement demonstrate persistent bone marrow hyperintensity on high-*b*-value images, which is suggestive of persistent tumor hypercellularity. The clear clinical value of DW MR imaging over that achieved with conventional T1- and T2-weighted spin-echo sequences perhaps best highlights the advantages of whole-body DW imaging for monitoring bone marrow response to therapy.

The data for the use of DW imaging to monitor metastatic bone disease are reinforced by observations in primary bone tumors such as osteogenic and Ewing sarcomas. MR imaging assessments of the response of osteosarcomas to neoadjuvant chemotherapy are problematic, because the tumors do not substantially reduce in size and may even increase in size (116). Successful chemotherapeutic response is gauged by the extent of tumor necrosis seen on resection specimens. Several investigators (60,116–118) have shown that there are significant differences in ADCs between patients who respond to treatment (with higher tumor ADCs after therapy) than in patients who do not respond to treatment.

On occasion, when there is tumor necrosis in the bone marrow, the signal intensity may remain persistently high despite successful treatment, owing to T2 shine-through or T1 value effects (Fig 3). This has been noted particularly in patients with multiple myeloma or lymphoma and occasionally in patients with other solid metastatic neoplasms. T2 shine-through effects are relatively easy to detect on ADC maps (very high values) and on T2-weighted or short tau inversion-recovery sequences. Thus, for lesions that are persistently hyperintense after therapy, it is necessary to review ADC maps and anatomic images before definite response assessments are made.

The long-term changes on whole-body DW images of bone marrow lesions that have been successfully treated are yet to be completely defined. Signal intensity and ADCs have been noted to decrease slowly, becoming visible many months after the start of therapy (20,137), depending on the type of tumor and therapy administered. The timelines of signal intensity and ADC changes with bone marrow healing still remain to be fully defined, as do the underlying pathophysiologic mechanisms. It is likely that bone sclerosis, removal of dead tumor cells, repopulation with normal marrow elements (including the reemergence of yellow bone marrow) (138), secondary chemotherapy-related myelofibrosis, tissue dehydration, and reduced perfusion all contribute to long-term reductions in signal intensities and ADCs.

Research and development perspectives.—Further research and development perspectives regarding therapy response are as follows:

1. Bone metastases that do not respond to cytotoxic therapy can show a slight increase (139), stability, or a decrease in ADC. The biophysical causes and limits for these ADC changes and the corresponding signal intensity appearances definitely require clarification for clinical deployment and drug development.

2. The range of ADCs in untreated nonnecrotic bone metastases needs to be documented to define the upper cutoff beyond which a successful treatment effect can be said to be present. The influences of imaging protocol and tumor type on such cutoff ADCs definitely need to be defined for clinical deployment and drug development.

3. It is not clear what proportion of tumor cells have to be killed or what the pattern of cell death must be (isolated scattered cell death vs confluent cell death) for ADC changes to become detectable on DW MR images. Clarification of this could be clinically important.

4. There is poor documentation on the reproducibility of whole-body DW imaging (ie, how much change is real for a given patient). It is also unclear what machine, patient, and analysis factors affect the measured reproducibility. This information is essential for the development of whole-body DW imaging as a pharmacodynamic biomarker for use in drug trials.

5. There is no documentation, to our knowledge, of the extent to which changes in DW MR imaging biomarkers result in patient benefit, as gauged by improvements in symptoms and survival for the variety of available therapies. This information is essential for the development of whole-body DW imaging as a tool for personalized medicine.

6. Concerning bone marrow response, it is not clear how quickly ADC increases occur in responders and the extent of ADC changes in relation to different treatments (chemotherapy vs radiation therapy vs hormone therapy). This information is a definite requirement for clinical deployment and drug development.

7. The timelines of signal intensity and ADC changes that accompany bone marrow healing still remain to be defined, as do the underlying pathophysiologic mechanisms. These are definite requirements for clinical deployment and drug development.

8. The relative contribution of whole-body DW imaging in comparison with other whole-body imaging techniques such as CT, conventional MR imaging, and PET (with its varieties of tracers) and bone scintigraphy in a variety of clinical scenarios involving therapy assessments are required. This knowledge could be clinically important.

Measurement Variability

When considering the clinical utility of DW MR imaging for the characterization of a tissue by means of the measurement of ADC, it is necessary to consider the interobserver and intraobserver variability of the manual method of measurements. This is particularly true when evaluating the nature of small structures, such as in the determination of nodal involvement by cancer. The variability of ADC measurements needs to be compared with the mean difference between malignant and benign nodes. This aspect has not been comprehensively assessed, but in one study the coefficient of reproducibility for normal nodal ADC measurements in volunteers without cancer was estimated to be about 13%–27% (±150 and ±310 μm^2/sec) for lymph nodes 5 mm or larger in diameter or those less than 5 mm (99). The interobserver variability of ADC measurement was as large as the intraobserver variability, which suggests that manual ADC measurements may not be sufficiently robust in daily practice for the evaluation of lymph nodes and is an argument for the development of software tools to enable automatic segmentation and ADC calculation for nodal assessment.

To be able to use ADC and tumor volume as response biomarkers in pharmaceutical trials, assessments of measurement error are needed. Estimates of reproducibility enable us to decide the minimal level of change that can be considered "real" for both patients and individuals. Tumor test-retest assessments in the absence of therapy are needed for this evaluation. For DW MR imaging, this can be undertaken by using the so-called coffee break examination approach wherein patients are studied twice, with repositioning between studies. An alternative approach sometimes reported in the literature is to obtain the measurement variability of normal tissues from pre- and post-therapy examinations and then to assume that the normal tissue (eg, muscle) will not have been changed by the therapy administered; this normal tissue threshold can then be used to determine the effects of tumor therapy (20,119). The measured difference in ADCs between pairs of examinations includes factors such as the natural biologic variability of the parameter, the variability inherent in the MR imaging system, and the additional errors introduced by appraisers or analysis methods, which, as we have noted, can be considerable for small structures (99). There have been relatively few published studies that document the reproducibility of DW MR imaging outside the brain, and most published studies are from institutions with considerable technical expertise (83,94,95); there are few larger scale multicenter studies (96). A generally applicable threshold for ADC change in extracranial applications of the whole-body DW imaging technique has not yet been established.

Reproducibility information needs to be combined with the expected magnitude of therapeutic effects, so as to allow determination of whether ADC change will be a useful tool. Data in the literature show that early ADC increases in response to therapeutic interventions may be of small magnitude. For example, Cui et al (68) studied liver metastases from stomach and colorectal cancers and observed ADC changes 3 and 7 days after the first dose of chemotherapy. Mean ADC increases from baseline values were approximately 25% in responding patients (quartiles, approximately +10 to +40%) and 8%–10% increases (quartiles, approximately −10% to +25%) in nonresponding patients. These changes are of relatively small magnitude compared with the expected reproducibility of the technique. The ability to confidently detect small increases in ADC may not be useful with regard to personalized medicine for patients with bone metastases. This is because increases in ADC may be seen in responders and nonresponders; the important point to remember is that ADC increases in nonresponders may be modest, whereas ADC changes in responders are usually larger (139).

To use whole-body DW imaging for personalized medicine, it is also important to determine how much of an increase in ADC results in patient benefit, as gauged by improvements in symptoms and survival. Concerning the latter, it may be that relative changes (expressed as percentage increase in ADC) are less powerful than the proportion of tumor pixels that exceed a threshold value for ADC, with the threshold representing the presence of dying cells and therapy-induced necrosis. Such thresholds have not yet been established for soft-tissue and bone metastases (see the list above in Bone Marrow Response).

Indications for Whole-Body DW Imaging

The use of whole-body DW imaging has not yet been proved to affect meaningful health outcomes in patients with metastatic cancer. There are no conclusive data in the published, peer-reviewed, medical literature to indicate that knowledge gained from whole-body DW imaging can be used to alter the therapy that is offered to patients and improve outcomes. In addition, no head-to-head trials have demonstrated that this technology provides tumor markers that are equal to or better than those from any existing methods in terms of efficacy

and clinical utility. Thus, although the roles of whole-body DW imaging in patient care are not as yet defined, the technology is certainly interesting enough to begin to pursue in the clinic so as to determine its possible roles.

In our opinion, scenarios in which DW MR imaging should be considered include the evaluation of cancer patients when there is a need to minimize radiation exposure (children and pregnant women) (3), cases where contrast-enhanced body CT evaluations are of inadequate quality (patients with renal failure, poor venous access, contrast medium allergies), or cases when there is a need to survey the entire bone marrow at a time of a world-wide shortage of technetium 99m (140). When evaluating the potential roles for whole-body DW imaging, it is important to examine patients with the appropriate histomorphologic cellular characteristics, preferably tumors with small-sized neoplastic cells such as multiple myeloma, neuroendocrine tumors, childhood tumors, melanoma, and small cell cancers. We have also found whole-body DW imaging to be useful in assessing therapy response in patients with mixed lytic and sclerotic metastatic bone disease (particularly from breast and prostate cancers).

Conclusions

DW MR imaging is emerging as a powerful clinical tool for directing the care of patients with cancer. Whole-body DW imaging can be clinically useful for disease detection, lesion characterization, and therapy response. Whole-body DW imaging is almost at the stage where it can enter widespread clinical investigations, because the technology is stable and protocols can be implemented on the majority of modern high-field-strength MR systems. We are now at the point where we can begin to define more clearly the potential roles for whole-body DW imaging by identifying clinical and pharmaceutical needs that it may be able to address. Whole-body DW imaging excels at bone marrow assessment for diagnosis and for therapy evaluation, where it can potentially address unmet clinical and pharmaceutical needs for a reliable measure of tumor response. Bone disease areas where whole-body DW imaging could make a substantial impact include therapy assessment in patients with metastatic breast or prostate cancer, as well as in patients with myeloma. There are pressing needs to document and understand the relationships between the mechanisms of action of treatments and the appearances on whole-body DW images. Therapy response criteria need to be established so that they can be then be tested in prospective clinical studies that incorporate conventional measures of patient benefit. We can also begin the process of defining how cancer care pathways would need to be altered to accommodate this new technology, to learn if there are improvements in cancer care. Until these steps are undertaken, DW MR imaging will not allow personalization of cancer care.

Disclosures of Potential Conflicts of Interest: A.R.P. Financial activities related to the present article: Siemens Healthcare provided support for travel to meetings for education purposes. Financial activities not related to the present article: is a member of the advisory board of Siemens Healthcare; has received software under a loan agreement from Siemens Healthcare. Other relationships: none to disclose. **D.M.K.** No financial activities to disclose. **D.J.C.** No financial activities to disclose.

References

1. Schaefer JF, Schlemmer HP. Total-body MR-imaging in oncology. Eur Radiol 2006; 16(9):2000–2015.
2. Schmidt GP, Reiser MF, Baur-Melnyk A. Whole-body MRI for the staging and follow-up of patients with metastasis. Eur J Radiol 2009;70(3):393–400.
3. Smith-Bindman R. Is computed tomography safe? N Engl J Med 2010;363(1):1–4.
4. Padhani AR, Liu G, Koh DM, et al. Diffusion-weighted magnetic resonance imaging as a cancer biomarker: consensus and recommendations. Neoplasia 2009;11(2):102–125.
5. Kwee TC, Takahara T, Ochiai R, et al. Whole-body diffusion-weighted magnetic resonance imaging. Eur J Radiol 2009;70(3): 409–417.
6. Koh DM, Collins DJ. Diffusion-weighted MRI in the body: applications and challenges in oncology. AJR Am J Roentgenol 2007;188(6):1622–1635.
7. Thoeny HC, De Keyzer F. Extracranial applications of diffusion-weighted magnetic resonance imaging. Eur Radiol 2007;17(6): 1385–1393.
8. Patterson DM, Padhani AR, Collins DJ. Technology insight: water diffusion MRI—a potential new biomarker of response to cancer therapy. Nat Clin Pract Oncol 2008; 5(4):220–233.
9. Takahara T, Imai Y, Yamashita T, Yasuda S, Nasu S, Van Cauteren M. Diffusion weighted whole body imaging with background body signal suppression (DWIBS): technical improvement using free breathing, STIR and high resolution 3D display. Radiat Med 2004;22(4):275–282.
10. Ohno Y, Koyama H, Onishi Y, et al. Non-small cell lung cancer: whole-body MR examination for M-stage assessment—utility for whole-body diffusion-weighted imaging compared with integrated FDG PET/CT. Radiology 2008;248(2):643–654.
11. Takenaka D, Ohno Y, Matsumoto K, et al. Detection of bone metastases in non-small cell lung cancer patients: comparison of whole-body diffusion-weighted imaging (DWI), whole-body MR imaging without and with DWI, whole-body FDG-PET/CT, and bone scintigraphy. J Magn Reson Imaging 2009; 30(2):298–308.
12. Taouli B, Koh DM. Diffusion-weighted MR imaging of the liver. Radiology 2010;254(1): 47–66.
13. Messiou C, Collins DJ, Morgan VA, Desouza NM. Optimising diffusion weighted MRI for imaging metastatic and myeloma bone disease and assessing reproducibility. Eur Radiol 2011;21(8):1713–1718.
14. Koh DM, Blackledge M, Collins DJ, et al. Reproducibility and changes in the apparent diffusion coefficients of solid tumours treated with combretastatin A4 phosphate and bevacizumab in a two-centre phase I clinical trial. Eur Radiol 2009;19(11):2728–2738.
15. Parikh T, Drew SJ, Lee VS, et al. Focal liver lesion detection and characterization with diffusion-weighted MR imaging: comparison with standard breath-hold T2-weighted imaging. Radiology 2008;246(3): 812–822.
16. Pope WB, Kim HJ, Huo J, et al. Recurrent glioblastoma multiforme: ADC histogram analysis predicts response to bevacizumab treatment. Radiology 2009;252(1):182–189.
17. Nowosielski M, Recheis W, Goebel G, et al. ADC histograms predict response to anti-angiogenic therapy in patients with recurrent high-grade glioma. Neuroradiology 2011;53(4):291–302.

18. Rose CJ, Mills SJ, O'Connor JP, et al. Quantifying spatial heterogeneity in dynamic contrast-enhanced MRI parameter maps. Magn Reson Med 2009;62(2):488–499.

19. Galbán CJ, Chenevert TL, Meyer CR, et al. The parametric response map is an imaging biomarker for early cancer treatment outcome. Nat Med 2009;15(5):572–576.

20. Reischauer C, Froehlich JM, Koh DM, et al. Bone metastases from prostate cancer: assessing treatment response by using diffusion-weighted imaging and functional diffusion maps—initial observations. Radiology 2010; 257(2):523–531.

21. Hwang S, Panicek DM. Magnetic resonance imaging of bone marrow in oncology, Part 1. Skeletal Radiol 2007;36(10):913–920.

22. Laor T, Jaramillo D. MR imaging insights into skeletal maturation: what is normal? Radiology 2009;250(1):28–38.

23. Goodsitt MM, Hoover P, Veldee MS, Hsueh SL. The composition of bone marrow for a dual-energy quantitative computed tomography technique. A cadaver and computer simulation study. Invest Radiol 1994;29(7): 695–704.

24. Vogler JB 3rd, Murphy WA. Bone marrow imaging. Radiology 1988;168(3):679–693.

25. Schellinger D, Lin CS, Fertikh D, et al. Normal lumbar vertebrae: anatomic, age, and sex variance in subjects at proton MR spectroscopy—initial experience. Radiology 2000;215(3):910–916.

26. Syed FA, Oursler MJ, Hefferanm TE, Peterson JM, Riggs BL, Khosla S. Effects of estrogen therapy on bone marrow adipocytes in postmenopausal osteoporotic women. Osteoporos Int 2008;19(9):1323–1330.

27. Ballon D, Watts R, Dyke JP, et al. Imaging therapeutic response in human bone marrow using rapid whole-body MRI. Magn Reson Med 2004;52(6):1234–1238.

28. Fletcher BD, Wall JE, Hanna SL. Effect of hematopoietic growth factors on MR images of bone marrow in children undergoing chemotherapy. Radiology 1993;189(3): 745–751.

29. Hobbs SK, Shi G, Homer R, Harsh G, Atlas SW, Bednarski MD. Magnetic resonance image-guided proteomics of human glioblastoma multiforme. J Magn Reson Imaging 2003;18(5):530–536.

30. Kiricuta IC, Simplăceanu V. Tissue water content and nuclear magnetic resonance in normal and tumor tissues. Cancer Res 1975; 35(5):1164–1167.

31. Manenti G, Di Roma M, Mancino S, et al. Malignant renal neoplasms: correlation between ADC values and cellularity in diffusion weighted magnetic resonance imaging at 3 T. Radiol Med (Torino) 2008;113(2): 199–213.

32. Hayashida Y, Hirai T, Morishita S, et al. Diffusion-weighted imaging of metastatic brain tumors: comparison with histologic type and tumor cellularity. AJNR Am J Neuroradiol 2006;27(7):1419–1425.

33. Humphries PD, Sebire NJ, Siegel MJ, Olsen OE. Tumors in pediatric patients at diffusion-weighted MR imaging: apparent diffusion coefficient and tumor cellularity. Radiology 2007;245(3):848–854.

34. Zelhof B, Pickles M, Liney G, et al. Correlation of diffusion-weighted magnetic resonance data with cellularity in prostate cancer. BJU Int 2009;103(7):883–888.

35. Liu Y, Bai R, Sun H, Liu H, Wang D. Diffusion-weighted magnetic resonance imaging of uterine cervical cancer. J Comput Assist Tomogr 2009;33(6):858–862.

36. Sugahara T, Korogi Y, Kochi M, et al. Usefulness of diffusion-weighted MRI with echo-planar technique in the evaluation of cellularity in gliomas. J Magn Reson Imaging 1999;9(1):53–60.

37. Lyng H, Haraldseth O, Rofstad EK. Measurement of cell density and necrotic fraction in human melanoma xenografts by diffusion weighted magnetic resonance imaging. Magn Reson Med 2000;43(6):828–836.

38. Ellingson BM, Malkin MG, Rand SD, et al. Validation of functional diffusion maps (fDMs) as a biomarker for human glioma cellularity. J Magn Reson Imaging 2010;31(3):538–548.

39. Guo AC, Cummings TJ, Dash RC, Provenzale JM. Lymphomas and high-grade astrocytomas: comparison of water diffusibility and histologic characteristics. Radiology 2002; 224(1):177–183.

40. Matsubayashi RN, Fujii T, Yasumori K, Muranaka T, Momosaki S. Apparent diffusion coefficient in invasive ductal breast carcinoma: correlation with detailed histologic features and the enhancement ratio on dynamic contrast-enhanced MR images. J Oncol 2010;2010. pii:821048. Epub 2010 Sep 2.

41. Wang Y, Chen ZE, Yaghmai V, et al. Diffusion-weighted MR imaging in pancreatic endocrine tumors correlated with histopathologic characteristics. J Magn Reson Imaging 2011;33(5):1071–1079.

42. Nonomura Y, Yasumoto M, Yoshimura R, et al. Relationship between bone marrow cellularity and apparent diffusion coefficient. J Magn Reson Imaging 2001;13(5): 757–760.

43. Tang GY, Lv ZW, Tang RB, et al. Evaluation of MR spectroscopy and diffusion-weighted MRI in detecting bone marrow changes in postmenopausal women with osteoporosis. Clin Radiol 2010;65(5):377–381.

44. Hillengass J, Bäuerle T, Bartl R, et al. Diffusion-weighted imaging for non-invasive and quantitative monitoring of bone marrow infiltration in patients with monoclonal plasma cell disease: a comparative study with histology. Br J Haematol 2011;153(6): 721–728.

45. Chan JH, Peh WC, Tsui EY, et al. Acute vertebral body compression fractures: discrimination between benign and malignant causes using apparent diffusion coefficients. Br J Radiol 2002;75(891):207–214.

46. Chen WT, Shih TT, Chen RC, et al. Vertebral bone marrow perfusion evaluated with dynamic contrast-enhanced MR imaging: significance of aging and sex. Radiology 2001;220(1):213–218.

47. Chen WT, Shih TT, Chen RC, et al. Blood perfusion of vertebral lesions evaluated with gadolinium-enhanced dynamic MRI: in comparison with compression fracture and metastasis. J Magn Reson Imaging 2002; 15(3):308–314.

48. Pui MH, Mitha A, Rae WI, Corr P. Diffusion-weighted magnetic resonance imaging of spinal infection and malignancy. J Neuroimaging 2005;15(2):164–170.

49. Wang XZ, Wang B, Gao ZQ, et al. Diffusion-weighted imaging of prostate cancer: correlation between apparent diffusion coefficient values and tumor proliferation. J Magn Reson Imaging 2009;29(6):1360–1366.

50. Calvar JA, Meli FJ, Romero C, et al. Characterization of brain tumors by MRS, DWI and Ki-67 labeling index. J Neurooncol 2005;72(3):273–280.

51. Arvinda HR, Kesavadas C, Sarma PS, et al. Glioma grading: sensitivity, specificity, positive and negative predictive values of diffusion and perfusion imaging. J Neurooncol 2009;94(1):87–96.

52. Woodfield CA, Tung GA, Grand DJ, Pezzullo JA, Machan JT, Renzulli JF 2nd. Diffusion-weighted MRI of peripheral zone prostate cancer: comparison of tumor apparent diffusion coefficient with Gleason score and percentage of tumor on core biopsy. AJR Am J Roentgenol 2010;194(4): W316–W322.

53. Tamada T, Sone T, Jo Y, et al. Apparent diffusion coefficient values in peripheral and transition zones of the prostate: comparison between normal and malignant prostatic tissues and correlation with histologic

grade. J Magn Reson Imaging 2008;28(3):720–726.

54. Sandrasegaran K, Sundaram CP, Ramaswamy R, et al. Usefulness of diffusion-weighted imaging in the evaluation of renal masses. AJR Am J Roentgenol 2010;194(2):438–445.

55. Turkbey B, Shah VP, Pang Y, et al. Is apparent diffusion coefficient associated with clinical risk scores for prostate cancers that are visible on 3-T MR images? Radiology 2011;258(2):488–495.

56. Hambrock T, Somford DM, Huisman HJ, et al. Relationship between apparent diffusion coefficients at 3.0-T MR imaging and Gleason grade in peripheral zone prostate cancer. Radiology 2011;259(2):453–461.

57. Geschwind JF, Artemov D, Abraham S, et al. Chemoembolization of liver tumor in a rabbit model: assessment of tumor cell death with diffusion-weighted MR imaging and histologic analysis. J Vasc Interv Radiol 2000;11(10):1245–1255.

58. Lang P, Wendland MF, Saeed M, et al. Osteogenic sarcoma: noninvasive in vivo assessment of tumor necrosis with diffusion-weighted MR imaging. Radiology 1998;206(1):227–235.

59. Deng J, Rhee TK, Sato KT, et al. In vivo diffusion-weighted imaging of liver tumor necrosis in the VX2 rabbit model at 1.5 Tesla. Invest Radiol 2006;41(4):410–414.

60. Uhl M, Saueressig U, van Buiren M, et al. Osteosarcoma: preliminary results of in vivo assessment of tumor necrosis after chemotherapy with diffusion- and perfusion-weighted magnetic resonance imaging. Invest Radiol 2006;41(8):618–623.

61. Kim H, Morgan DE, Zeng H, et al. Breast tumor xenografts: diffusion-weighted MR imaging to assess early therapy with novel apoptosis-inducing anti-DR5 antibody. Radiology 2008;248(3):844–851.

62. Liimatainen T, Hakumäki JM, Kauppinen RA, Ala-Korpela M. Monitoring of gliomas in vivo by diffusion MRI and (1)H MRS during gene therapy-induced apoptosis: interrelationships between water diffusion and mobile lipids. NMR Biomed 2009;22(3):272–279.

63. Nakajo M, Kajiya Y, Kaneko T, et al. FDG PET/CT and diffusion-weighted imaging for breast cancer: prognostic value of maximum standardized uptake values and apparent diffusion coefficient values of the primary lesion. Eur J Nucl Med Mol Imaging 2010;37(11):2011–2020.

64. Razek AA, Gaballa G, Denewer A, Nada N. Invasive ductal carcinoma: correlation of apparent diffusion coefficient value with pathological prognostic factors. NMR Biomed 2010;23(6):619–623.

65. Razek AA, Fathy A, Gawad TA. Correlation of apparent diffusion coefficient value with prognostic parameters of lung cancer. J Comput Assist Tomogr 2011;35(2):248–252.

66. Roth Y, Tichler T, Kostenich G, et al. High-b-value diffusion-weighted MR imaging for pretreatment prediction and early monitoring of tumor response to therapy in mice. Radiology 2004;232(3):685–692.

67. Koh DM, Scurr E, Collins D, et al. Predicting response of colorectal hepatic metastasis: value of pretreatment apparent diffusion coefficients. AJR Am J Roentgenol 2007;188(4):1001–1008.

68. Cui Y, Zhang XP, Sun YS, Tang L, Shen L. Apparent diffusion coefficient: potential imaging biomarker for prediction and early detection of response to chemotherapy in hepatic metastases. Radiology 2008;248(3):894–900.

69. Sun YS, Zhang XP, Tang L, et al. Locally advanced rectal carcinoma treated with preoperative chemotherapy and radiation therapy: preliminary analysis of diffusion-weighted MR imaging for early detection of tumor histopathologic downstaging. Radiology 2010;254(1):170–178.

70. Dewhirst MW, Cao Y, Moeller B. Cycling hypoxia and free radicals regulate angiogenesis and radiotherapy response. Nat Rev Cancer 2008;8(6):425–437.

71. Höckel M, Vaupel P. Tumor hypoxia: definitions and current clinical, biologic, and molecular aspects. J Natl Cancer Inst 2001;93(4):266–276.

72. Niwa T, Ueno M, Ohkawa S, et al. Advanced pancreatic cancer: the use of the apparent diffusion coefficient to predict response to chemotherapy. Br J Radiol 2009;82(973):28–34.

73. Thoeny HC, De Keyzer F, Chen F, et al. Diffusion-weighted MR imaging in monitoring the effect of a vascular targeting agent on rhabdomyosarcoma in rats. Radiology 2005;234(3):756–764.

74. Thoeny HC, De Keyzer F, Chen F, et al. Diffusion-weighted magnetic resonance imaging allows noninvasive in vivo monitoring of the effects of combretastatin a-4 phosphate after repeated administration. Neoplasia 2005;7(8):779–787.

75. Fischer MA, Nanz D, Hany T, et al. Diagnostic accuracy of whole-body MRI/DWI image fusion for detection of malignant tumours: a comparison with PET/CT. Eur Radiol 2011;21(2):246–255.

76. Wu LM, Gu HY, Zheng J, et al. Diagnostic value of whole-body magnetic resonance imaging for bone metastases: a systematic review and meta-analysis. J Magn Reson Imaging 2011;34(1):128–135.

77. Chen W, Jian W, Li HT, et al. Whole-body diffusion-weighted imaging vs. FDG-PET for the detection of non-small-cell lung cancer. How do they measure up? Magn Reson Imaging 2010;28(5):613–620.

78. Abdulqadhr G, Molin D, Aström G, et al. Whole-body diffusion-weighted imaging compared with FDG-PET/CT in staging of lymphoma patients. Acta Radiol 2011;52(2):173–180.

79. Heusner TA, Kuemmel S, Koeninger A, et al. Diagnostic value of diffusion-weighted magnetic resonance imaging (DWI) compared to FDG PET/CT for whole-body breast cancer staging. Eur J Nucl Med Mol Imaging 2010;37(6):1077–1086.

80. Kwee TC, Takahara T, Vermoolen MA, Bierings MB, Mali WP, Nievelstein RA. Whole-body diffusion-weighted imaging for staging malignant lymphoma in children. Pediatr Radiol 2010;40(10):1592–1602; quiz 1720–1721.

81. Wang H, Cheng L, Zhang X, et al. Renal cell carcinoma: diffusion-weighted MR imaging for subtype differentiation at 3.0 T. Radiology 2010;257(1):135–143.

82. Paudyal B, Paudyal P, Tsushima Y, et al. The role of the ADC value in the characterisation of renal carcinoma by diffusion-weighted MRI. Br J Radiol 2010;83(988):336–343.

83. Inada Y, Matsuki M, Nakai G, et al. Body diffusion-weighted MR imaging of uterine endometrial cancer: is it helpful in the detection of cancer in nonenhanced MR imaging? Eur J Radiol 2009;70(1):122–127.

84. Gutzeit A, Doert A, Froehlich JM, et al. Comparison of diffusion-weighted whole body MRI and skeletal scintigraphy for the detection of bone metastases in patients with prostate or breast carcinoma. Skeletal Radiol 2010;39(4):333–343.

85. Eiber M, Holzapfel K, Ganter C, et al. Whole-body MRI including diffusion-weighted imaging (DWI) for patients with recurring prostate cancer: technical feasibility and assessment of lesion conspicuity in DWI. J Magn Reson Imaging 2011;33(5):1160–1170.

86. Costelloe CM, Chuang HH, Madewell JE, Ueno NT. Cancer response criteria and bone metastases: RECIST 1.1, MDA and PERCIST. J Cancer 2010;1:80–92.

87. Yabuuchi H, Matsuo Y, Kamitani T, et al. Parotid gland tumors: can addition of diffusion-weighted MR imaging to dynamic

contrast-enhanced MR imaging improve diagnostic accuracy in characterization? Radiology 2008;249(3):909–916.

88. Lin C, Luciani A, Itti E, et al. Whole-body diffusion-weighted magnetic resonance imaging with apparent diffusion coefficient mapping for staging patients with diffuse large B-cell lymphoma. Eur Radiol 2010; 20(8):2027–2038.

89. Lin G, Ho KC, Wang JJ, et al. Detection of lymph node metastasis in cervical and uterine cancers by diffusion-weighted magnetic resonance imaging at 3T. J Magn Reson Imaging 2008;28(1):128–135.

90. Holzapfel K, Duetsch S, Fauser C, Eiber M, Rummeny EJ, Gaa J. Value of diffusion-weighted MR imaging in the differentiation between benign and malignant cervical lymph nodes. Eur J Radiol 2009;72(3):381–387.

91. Nomori H, Mori T, Ikeda K, et al. Diffusion-weighted magnetic resonance imaging can be used in place of positron emission tomography for N staging of non-small cell lung cancer with fewer false-positive results. J Thorac Cardiovasc Surg 2008;135(4): 816–822.

92. Eiber M, Beer AJ, Holzapfel K, et al. Preliminary results for characterization of pelvic lymph nodes in patients with prostate cancer by diffusion-weighted MR-imaging. Invest Radiol 2010;45(1):15–23.

93. Dirix P, Vandecaveye V, De Keyzer F, et al. Diffusion-weighted MRI for nodal staging of head and neck squamous cell carcinoma: impact on radiotherapy planning. Int J Radiat Oncol Biol Phys 2010;76(3):761–766.

94. Nakayama J, Miyasaka K, Omatsu T, et al. Metastases in mediastinal and hilar lymph nodes in patients with non-small cell lung cancer: quantitative assessment with diffusion-weighted magnetic resonance imaging and apparent diffusion coefficient. J Comput Assist Tomogr 2010;34(1):1–8.

95. Chen YB, Liao J, Xie R, Chen GL, Chen G. Discrimination of metastatic from hyperplastic pelvic lymph nodes in patients with cervical cancer by diffusion-weighted magnetic resonance imaging. Abdom Imaging 2011;36(1):102–109.

96. Perrone A, Guerrisi P, Izzo L, et al. Diffusion-weighted MRI in cervical lymph nodes: differentiation between benign and malignant lesions. Eur J Radiol 2011;77(2):281–286.

97. Koşucu P, Tekinbaş C, Erol M, et al. Mediastinal lymph nodes: assessment with diffusion-weighted MR imaging. J Magn Reson Imaging 2009;30(2):292–297.

98. Vandecaveye V, De Keyzer F, Vander Poorten V, et al. Head and neck squamous cell carcinoma: value of diffusion-weighted MR imaging for nodal staging. Radiology 2009; 251(1):134–146.

99. Kwee TC, Takahara T, Luijten PR, Nievelstein RA. ADC measurements of lymph nodes: inter- and intra-observer reproducibility study and an overview of the literature. Eur J Radiol 2010;75(2):215–220.

100. Kim SH, Kim SC, Choi BI, Han MC. Uterine cervical carcinoma: evaluation of pelvic lymph node metastasis with MR imaging. Radiology 1994;190(3):807–811.

101. Nakai G, Matsuki M, Inada Y, et al. Detection and evaluation of pelvic lymph nodes in patients with gynecologic malignancies using body diffusion-weighted magnetic resonance imaging. J Comput Assist Tomogr 2008;32(5):764–768.

102. Roy C, Bierry G, Matau A, Bazille G, Pasquali R. Value of diffusion-weighted imaging to detect small malignant pelvic lymph nodes at 3 T. Eur Radiol 2010;20(8): 1803–1811.

103. Thoeny HC, Triantafyllou M, Birkhaeuser FD, et al. Combined ultrasmall superparamagnetic particles of iron oxide-enhanced and diffusion-weighted magnetic resonance imaging reliably detect pelvic lymph node metastases in normal-sized nodes of bladder and prostate cancer patients. Eur Urol 2009;55(4):761–769.

104. Mori T, Nomori H, Ikeda K, et al. Diffusion-weighted magnetic resonance imaging for diagnosing malignant pulmonary nodules/masses: comparison with positron emission tomography. J Thorac Oncol 2008; 3(4):358–364.

105. Ho KC, Lin G, Wang JJ, Lai CH, Chang CJ, Yen TC. Correlation of apparent diffusion coefficients measured by 3T diffusion-weighted MRI and SUV from FDG PET/CT in primary cervical cancer. Eur J Nucl Med Mol Imaging 2009;36(2):200–208.

106. Kwee TC, Takahara T, Ochiai R, et al. Complementary roles of whole-body diffusion-weighted MRI and 18F-FDG PET: the state of the art and potential applications. J Nucl Med 2010;51(10):1549–1558.

107. Padhani AR, Miles KA. Multiparametric imaging of tumor response to therapy. Radiology 2010;256(2):348–364.

108. Hamstra DA, Rehemtulla A, Ross BD. Diffusion magnetic resonance imaging: a biomarker for treatment response in oncology. J Clin Oncol 2007;25(26):4104–4109.

109. Thoeny HC, Ross BD. Predicting and monitoring cancer treatment response with diffusion-weighted MRI. J Magn Reson Imaging 2010;32(1):2–16.

110. Padhani AR, Koh DM. Diffusion MR imaging for monitoring of treatment response. Magn Reson Imaging Clin N Am 2011;19(1): 181–209.

111. Larocque MP, Syme A, Yahya A, Wachowicz K, Allalunis-Turner J, Fallone BG. Monitoring T2 and ADC at 9.4 T following fractionated external beam radiation therapy in a mouse model. Phys Med Biol 2010;55(5): 1381–1393.

112. Pickles MD, Gibbs P, Lowry M, Turnbull LW. Diffusion changes precede size reduction in neoadjuvant treatment of breast cancer. Magn Reson Imaging 2006;24(7):843–847.

113. Yankeelov TE, Lepage M, Chakravarthy A, et al. Integration of quantitative DCE-MRI and ADC mapping to monitor treatment response in human breast cancer: initial results. Magn Reson Imaging 2007;25(1):1–13.

114. Theilmann RJ, Borders R, Trouard TP, et al. Changes in water mobility measured by diffusion MRI predict response of metastatic breast cancer to chemotherapy. Neoplasia 2004;6(6):831–837.

115. Kamel IR, Liapi E, Reyes DK, Zahurak M, Bluemke DA, Geschwind JF. Unresectable hepatocellular carcinoma: serial early vascular and cellular changes after transarterial chemoembolization as detected with MR imaging. Radiology 2009;250(2):466–473.

116. Hayashida Y, Yakushiji T, Awai K, et al. Monitoring therapeutic responses of primary bone tumors by diffusion-weighted image: Initial results. Eur Radiol 2006; 16(12):2637–2643.

117. Uhl M, Saueressig U, Koehler G, et al. Evaluation of tumour necrosis during chemotherapy with diffusion-weighted MR imaging: preliminary results in osteosarcomas. Pediatr Radiol 2006;36(12):1306–1311.

118. Oka K, Yakushiji T, Sato H, Hirai T, Yamashita Y, Mizuta H. The value of diffusion-weighted imaging for monitoring the chemotherapeutic response of osteosarcoma: a comparison between average apparent diffusion coefficient and minimum apparent diffusion coefficient. Skeletal Radiol 2010;39(2):141–146.

119. Hamstra DA, Galbán CJ, Meyer CR, et al. Functional diffusion map as an early imaging biomarker for high-grade glioma: correlation with conventional radiologic response and overall survival. J Clin Oncol 2008;26(20):3387–3394.

120. Mardor Y, Pfeffer R, Spiegelmann R, et al. Early detection of response to radiation therapy in patients with brain malignancies using conventional and high b-value diffusion-weighted magnetic resonance imaging. J Clin Oncol 2003;21(6):1094–1100.

121. Dudeck O, Zeile M, Pink D, et al. Diffusion-weighted magnetic resonance imaging allows monitoring of anticancer treatment effects in patients with soft-tissue sarcomas. J Magn Reson Imaging 2008;27(5):1109–1113.

122. Jennings D, Hatton BN, Guo J, et al. Early response of prostate carcinoma xenografts to docetaxel chemotherapy monitored with diffusion MRI. Neoplasia 2002;4(3):255–262.

123. Jordan BF, Runquist M, Raghunand N, et al. Dynamic contrast-enhanced and diffusion MRI show rapid and dramatic changes in tumor microenvironment in response to inhibition of HIF-1alpha using PX-478. Neoplasia 2005;7(5):475–485.

124. Sharma U, Danishad KK, Seenu V, Jagannathan NR. Longitudinal study of the assessment by MRI and diffusion-weighted imaging of tumor response in patients with locally advanced breast cancer undergoing neoadjuvant chemotherapy. NMR Biomed 2009;22(1):104–113.

125. De Keyzer F, Vandecaveye V, Thoeny H, et al. Dynamic contrast-enhanced and diffusion-weighted MRI for early detection of tumoral changes in single-dose and fractionated radiotherapy: evaluation in a rat rhabdomyosarcoma model. Eur Radiol 2009;19(11):2663–2671.

126. Lee SC, Poptani H, Pickup S, et al. Early detection of radiation therapy response in non-Hodgkin's lymphoma xenografts by in vivo 1H magnetic resonance spectroscopy and imaging. NMR Biomed 2010;23(6):624–632.

127. Hamstra DA, Lee KC, Moffat BA, Chenevert TL, Rehemtulla A, Ross BD. Diffusion magnetic resonance imaging: an imaging treatment response biomarker to chemoradiotherapy in a mouse model of squamous cell cancer of the head and neck. Transl Oncol 2008;1(4):187–194.

128. Eccles CL, Haider EA, Haider MA, Fung S, Lockwood G, Dawson LA. Change in diffusion weighted MRI during liver cancer radiotherapy: preliminary observations. Acta Oncol 2009;48(7):1034–1043.

129. Kim S, Loevner L, Quon H, et al. Diffusion-weighted magnetic resonance imaging for predicting and detecting early response to chemoradiation therapy of squamous cell carcinomas of the head and neck. Clin Cancer Res 2009;15(3):986–994.

130. Galbán CJ, Mukherji SK, Chenevert TL, et al. A feasibility study of parametric response map analysis of diffusion-weighted magnetic resonance imaging scans of head and neck cancer patients for providing early detection of therapeutic efficacy. Transl Oncol 2009;2(3):184–190.

131. Hamstra DA, Chenevert TL, Moffat BA, et al. Evaluation of the functional diffusion map as an early biomarker of time-to-progression and overall survival in high-grade glioma. Proc Natl Acad Sci U S A 2005;102(46):16759–16764.

132. Liu Y, Bai R, Sun H, Liu H, Zhao X, Li Y. Diffusion-weighted imaging in predicting and monitoring the response of uterine cervical cancer to combined chemoradiation. Clin Radiol 2009;64(11):1067–1074.

133. Harry VN, Semple SI, Gilbert FJ, Parkin DE. Diffusion-weighted magnetic resonance imaging in the early detection of response to chemoradiation in cervical cancer. Gynecol Oncol 2008;111(2):213–220.

134. Dirix P, Vandecaveye V, De Keyzer F, Stroobants S, Hermans R, Nuyts S. Dose painting in radiotherapy for head and neck squamous cell carcinoma: value of repeated functional imaging with (18)F-FDG PET, (18)F-fluoromisonidazole PET, diffusion-weighted MRI, and dynamic contrast-enhanced MRI. J Nucl Med 2009;50(7):1020–1027.

135. Ballon D, Dyke J, Schwartz LH, et al. Bone marrow segmentation in leukemia using diffusion and T (2) weighted echo planar magnetic resonance imaging. NMR Biomed 2000;13(6):321–328.

136. Byun WM, Shin SO, Chang Y, Lee SJ, Finsterbusch J, Frahm J. Diffusion-weighted MR imaging of metastatic disease of the spine: assessment of response to therapy. AJNR Am J Neuroradiol 2002;23(6):906–912.

137. Messiou C, Collins D, Morgan V, et al. ADC changes with time in focal and diffuse myleoma bone disease as indicators of disease response and progression [abstr]. In: Proceedings of the Joint Meeting of the International Society for Magnetic Resonance in Medicine and the European Society for Magnetic Resonance in Medicine and Biology, Stockholm, 2010; 1716.

138. Messiou C, deSouza NM. Diffusion Weighted Magnetic Resonance Imaging of metastatic bone disease: A biomarker for treatment response monitoring. Cancer Biomark 2010;6(1):21–32.

139. Messiou C, Collins DJ, Giles S, de Bono JS, Bianchini D, de Souza NM. Assessing response in bone metastases in prostate cancer with diffusion weighted MRI. Eur Radiol 2011;21(10):2169–2177.

140. Ballinger JR. Short- and long-term responses to molybdenum-99 shortages in nuclear medicine. Br J Radiol 2010;83(995):899–901.